Journal of Materials Chemistry B

Accepted Manuscript

ROYAL SOCIETY OF CHEMISTRY

www.rsc.org/materialsB

Journal of Materials Chemistry B

ARTICLE

Single-step Electrospun TiO_2-Au Hybrid Electrodes for High Selectivity Photoelectrocatalytic Glutathione Bioanalysis

Received 00th January 20xx,
Accepted 00th January 20xx

DOI: 10.1039/x0xx00000x

www.rsc.org/

Anitha Devadoss,[a]† Asako Kuragano,[a,b] Chiaki Terashima,[a,c*] P. Sudhagar,[a]† Kazuya Nakata,[a,b,c] Takeshi Kondo,[a,b,c] Makoto Yuasa[a,b,c] and Akira Fujishima[a,c]

Understanding the fundamentals of photoelectrocatalytic (PEC) biomolecular oxidation benefits the development of next-generation PEC biosensors. In this work, we report the single-step electrospun TiO_2-Au hybrid nanofibers (HNF) as the potential candidate for PEC glutathione (GSH) bioanalysis. The chemical environment of TiO_2 and TiO_2-Au HNFs was studied with X-ray photoelectron spectroscopy (XPS) and found to have a strong electronic interaction between TiO_2 and Au NPs. The PEC measurements reveal that the intramolecular backbone hydrogen bonding of GSH molecules predominantly contributes highly active Au-GSH bio-nano interfaces, which facilitates the PEC oxidation rate of GSH and thus enhancing the photocurrent. Moreover, the presence of Au NPs acts as auxiliary electron transport channels resulting in enhanced charge collection at external circuit. As a result, TiO_2-Au electrode generated two fold higher photocurrent density of ~84.4 μAcm^{-2} in presence of 0.5 mM GSH, where the pristine TiO_2 NFs displayed only a negligible influence. Likewise, the TiO_2-Au HNFs electrode showed a higher sensitivity of 0.002 mM and a wide linear detection range between 0.022 mM to 0.7 mM, with a superior selectivity towards GSH bioanalysis over ascorbic acid and glucose at -0.33 V (vs. Ag/AgCl) than pristine TiO_2. The implications of these findings towards the development of next-generation PEC biosensor are discussed.

Introduction

Semiconductor photocatalysis integrates photoexcitation process and surface catalysis. The photoexcitation involves light absorption and charge carrier generation (e^- and h^+), while surface catalysis concerns the utilization of photogenerated carrier. Photocatalysis based semiconductor technology has attracted considerable research interest for the purpose of effectively utilizing the solar energy in solar cells, solar fuel cells, and organic pollutant removal etc.[1-4] In a different dimension, the photoelectrochemical (PEC) process has become a new and promising analytical tool for the detection of biomolecules.[5-8] Fujishima *et al.* explored that the light driven photosensitized water oxidation phenomenon[1] as a key tool for accessing photoholes at the valence band of semiconductor to advanced oxidation of chemical components in gas or in liquid phase. In this context, PEC oxidation of biomolecules by the photogenerated holes at valence band of semiconductor is an interesting approach for PEC bioanalysis.[9] In PEC biosensor, a charge transfer reaction (charge separation and recombination) between photoactive material and analyte under light irradiation plays a vital role in defining the sensitivity and selectivity. It is widely recognized that TiO_2 exhibits remarkable photoelectrocatalytic activity and chemical stability in neutral pH, which is the primary prerequisite for bioanalysis.[10, 11] Moreover, the key benefit of high positive valence band position of TiO_2 (~3 V vs NHE) compared to water oxidation potential ~1.2 V vs NHE, might extend the application of PEC bioanalysis to a wide range of biomolecules.[12]

Over the past decade, TiO_2 based bioanalysis demonstrated successful detection of various biomolecules. Recently, glutathione (GSH) bioanalysis is gaining momentum since GSH serves as a potential antioxidant against free radicals and thus, plays a central role in detoxification and biotransformation of chemotherapeutic drugs.[13] More specifically, in conjunction with the detoxification enzymes like glutathione peroxidase (GSH-Px), glutathione reductase, glutathione *S*-transferases (GST) etc. GSH detoxifies the effect of external toxic materials.[14, 15] In this line, cancer cells are known to have a higher concentration of GSH, which hinders the efficiency of anticancer therapy by detoxifying the carcinogens and by consuming toxic free radicals generated by therapy. Moreover, the physiological concentrations of GSH are an excellent indicator of various disease risks in human. As the elevated levels of GSH are closely associated with a number of diseases in humans including aging and cancer,[16-21] a number of methods including electrochemical,[22, 23] fluorescence[24] and luminescence[15], have been developed to

[a] *Photocatalysis International Research Center, Research Institute for Science & Technology, Tokyo University of Science, 2641 Yamazaki, Noda, Chiba 278-8510, JAPAN. *E-mail: terashima@rs.tus.ac.jp*
[b] *Faculty of Science and Technology, Tokyo University of Science, 2641 Yamazaki, Noda, Chiba 278-8510, JAPAN*
[c] *ACT-C/JST, 4-1-8 Honcho, Kawaguchi, Saitama, 333-0012, JAPAN*
† These authors contributed equally.
Electronic Supplementary Information (ESI) available: [XRD, XPS and JV Plots]. See DOI: 10.1039/x0xx00000x

interrogate the levels of GSH in blood. Conventional methods of monitoring the GSH expression such as fluorescence and electrochemical detection techniques suffer from photo-bleaching and high over potential, respectively.[25, 26] Thus, developing new technologies applicable for early and accurate detection of GSH expression at much lower potential is therefore of utmost importance in clinical diagnosis, treatment and prognosis of tumors.

In the past decade, a lot of research has been devoted on exploiting TiO_2 photoelectrodes for PEC bioanalysis.[27-29] With the aim of promoting the visible light accessing capability, TiO_2 is integrated with visible light band gap materials (CdSe, CdTe and carbon QDs),[30, 31] and/or doped with non-metals (nitrogen).[32] In this context, the first report on PEC based GSH bioanalysis using porphyrin sensitized TiO_2 nanoparticles electrode was reported by Tu *et al*.[33] Besides improving the weak visible light reception at electrodes modified with TiO_2 nanoparticles, porphyrin sensitization also promoted photo-excited charge carrier generation and thus reduced the onset potential of PEC GSH oxidation to ~0.2 V. Later, Tang *et al.* demonstrated the PEC GSH oxidation using vertically grown one-dimensional TiO_2 nanowires.[34] These 1-D TiO_2 nanowires were sensitized with 'hemin' and coated with co-catalyst (IrO_2 NPs). Here, the hemin promoted the selectivity of GSH targets, and the IrO_2 NPs effectively enhanced the charge transfer kinetics. As a result, the modified TiO_2 nanowire showed ~100% increase of photocurrent compared to the pristine TiO_2 NWs. Compared to the single-phase TiO_2 photocatalysis, TiO_2-Au heterostructures have shown higher photocurrent and increased charge separation.[35, 36] Here, the infusion of metal NPs promotes the PEC activity of TiO_2 since the unique band bending resulting from the formation of semiconductor-metal interface (Schottky junction) favors the separation of charge carriers. In general, the enhancement in photocurrent generation is attributed to the presence of Au NPs those act as "electron-sink" and thus reduces the charge recombination at TiO_2. We have recently reported that the direct assembly of Au NPs promoted the photocatalytic performance of TiO_2 nanowires due to the combined light scattering and reduced recombination.[4] On the other hand, it is also reported that the surface plasmon resonance (SPR) of Au NPs, originating from the collective oscillation of surface electrons upon visible light irradiation, enhances the photocatalytic activity of host metal oxide.[37-40] Recently, pre-synthesized powder-type Pt decorated TiO_2 nanowhisker also demonstrated successful GSH sensing.[41] Despite the reported biosensing performances, yet there is a great scope for sensitivity and selectivity improvement in PEC GSH bioanalysis through probing the nano-bio interfaces.

It is already known that the method of TiO_2-Au hybrid formation plays a significant role in controlling the activity of Au NPs. Priebe *et al*[42] showed that the method of Au deposition controls the TiO_2-Au electronic interface and thus, influences the photocatalytic reaction activity of TiO_2. Moreover, overloading of Au NPs exhibits detrimental light blocking effect at TiO_2 surface.[43] Therefore, it is necessary to clearly understand the nano-bio interface to fully exploit the PEC activity of TiO_2-Au hybrid nanomaterials for bioanalysis. With the ultimate goal of understanding the interactions at nano-bio interfaces, we have developed single step, ready-to-use TiO_2-Au hybrid nanofiber (HNF) electrodes using electrospinning technique for GSH bioanalysis. To the best of our knowledge, this is the first report on the PEC application of electrospun TiO_2-Au hybrid electrode for PEC GSH detection. Here, the feasibility of single-step fabrication of multiple complex materials or nanocomposites[44, 45] using electrospinning is exploited. Moreover, the main advantage of highly interconnected one dimensional (1-D) nanofibrous framework (rapid electron transport pathways and their wide pore channels) are anticipated to enhance the bioanalyte percolation that might result in effective electrode/electrolyte nano-bio interfaces.[46] The PEC measurements reveal the superior performance of TiO_2-Au HNFs over the pristine TiO_2. Although the existence of Au NPs are generally recognized to improve the PEC activity of TiO_2, this work is anticipated to provide new insights into the biomolecular selectivity perfections at nano-bio interfaces, that will open a new dimensionality in PEC bioanalysis.

Results and discussion

The mechanism of PEC glutathione bioanalysis at TiO_2-Au HNF electrodes is illustrated in **Scheme 1**. The typical photoelectrocatalytic biomolecular oxidation process at the photoanode (TiO_2-Au HNFs) is explained as follows: Upon solar light illumination, photogenerated charge carriers (e^- and h^+) are produced at TiO_2-Au HNFs. The photoelectrons are transported to charge collector (fluorinated tin oxide: FTO) through TiO_2 NF channels, whereas the photoholes are subsequently scavenged to the electrolyte interface, where the dispersed GSH molecules gets oxidized.

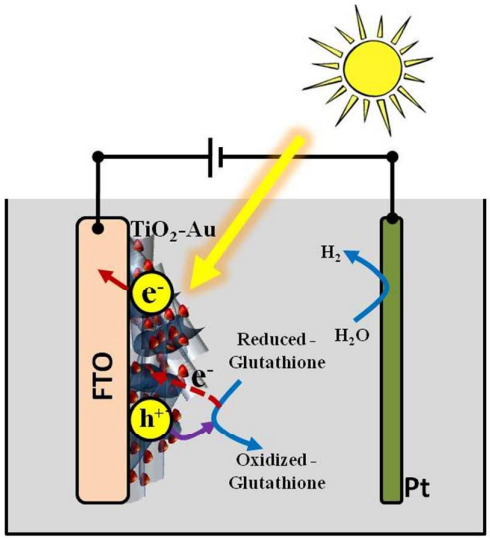

Scheme 1. Schematic illustration of photoelectrochemical cells for glutathione sensing using TiO_2-Au composite as photoanode and Pt wire serve as counter electrode.

Besides improving the visible light activity of TiO_2, the presence of Au NPs are anticipated to promote the adsorption

of GSH molecules onto TiO_2-Au, which could improve the GSH oxidation and thus, contributing additional oxidative electron to the circuit. During this process, GSH is oxidized into glutathione disulphide (GSSG). As the increase in the photocurrent solely depends on the GSH oxidation, the concentration of GSH can be precisely quantified from the photocurrent enhancements.

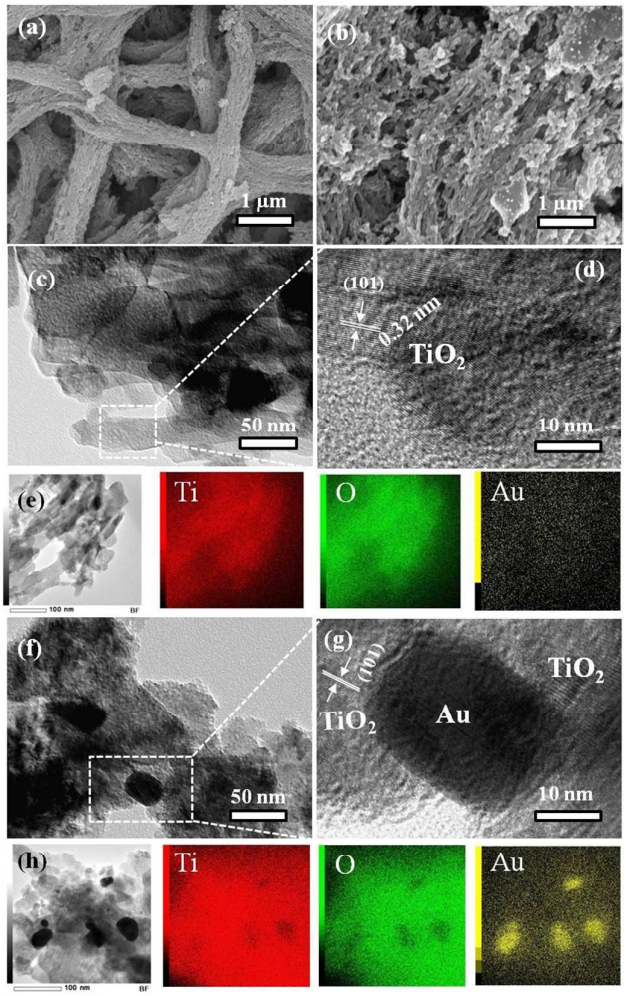

Figure 1. SEM images of (a) TiO_2 and (b) TiO_2-Au electrodes; TEM image of TiO_2 (c) at 50 nm scale and (d) high magnification at 10 nm scale; (e) elemental mapping of Ti,O, and Au at TiO_2 sample measured from Fig 2(c); High resolution TEM image of TiO_2-Au (f) at 50 nm scale and (g) high magnification at 10 nm scale; (h) elemental mapping of Ti, O, and Au at TiO_2-Au composite at TiO_2-Au sample Fig. 1(f).

The crystallite structure of electrospun TiO_2 and TiO_2-Au HNFs on conducting substrates were examined with XRD and the results are presented in **Fig.S1.** (See supporting information). From **Fig.S1**, the predominant peak observed at 25.3° in both samples confirm the (101) anatase crystallite phase. Remaining peaks witnessed at 37.6°, 47.6°, 53.8° and 54.8° corresponds to (004), (200) (105) and (211) crystallite phases of TiO_2 respectively (standard JCPDS of anatase TiO_2 (21-1272). The significant crystallite peaks related to Au does not exist in TiO_2-Au HNF electrode, which implies that Au NPs are impregnated at a very mild concentration in TiO_2. The existence of the Au NPs is further investigated by comparing the peak width (FWHM) values. It is inferred that the FWHM of TiO_2-Au crystallite peaks (101), (004) and (200) are narrower than pristine TiO_2, which ensures the presence of Au NPs at the TiO_2 lattice. The surface morphology and the elemental analysis of TiO_2 NFs and TiO_2-Au HNFs were examined with scanning electron microscopy (**Fig.1).** The pristine TiO_2 (**Fig.1a**) electrode depicts the presence of highly interconnected 1-D TiO_2 fiber bundles with a mean diameter of 500-700 nm. These TiO_2 NF bundles are found to be formed by connecting the individual TiO_2 NPs. This can be attributed to the removal of PVP species from as-synthesized TiO_2 NFs upon sintering at 500 °C, forming the porous sites that leads to the separation of individual spherical particles in the NF bundles.[47] Despite the similar fabrication conditions, TiO_2-Au electrode (**Fig. 1b**) shows the formation of thinner nanofibers compared to pristine TiO_2. This may be ascribed to the simultaneous crystallization of Au NPs and TiO_2 during sintering treatment; perhaps the PVP polymer species removal could facilitate the Au NPs diffusivity towards the porous sites at TiO_2 bundles. This process might transform the thick TiO_2 bundle into thinner bundles. For further analyzing the distribution of Au NPs in TiO_2 NFs, high magnification TEM images were recorded (**Fig.1 c, d and f, g**). The high magnification TEM image of TiO_2 electrode (**Fig. 1c**) ensures the interconnected structure of TiO_2 NFs assembled from individual TiO_2 NPs (**See supporting information Fig.S2**). From **Fig.1d**, the estimated lattice diameter of ~0.32 nm ensures the anatase TiO_2 (101) crystallite phase, which is in line with XRD results (**Fig.S1**). On the other hand, **Fig.1f** shows that Au NPs of ~15 nm in diameter are randomly incorporated in TiO_2 crystallite and **Fig.1g** clearly evinces that Au NP is bridging the TiO_2 crystals, which may be anticipated to enhance the charge transport along the TiO_2 channel. Elemental mapping on TiO_2 (**Fig.1e**) and TiO_2-Au (**Fig.1h**) samples confirm the presence of individual elements (Ti and O). In close proximity comparison between **Fig.1h** and **1e** strongly corroborate the presence of Au NPs only in TiO_2-Au sample. As discussed earlier, the one-step precursor (metal and metal oxide) derived TiO_2-Au composite NFs show effective incorporation of Au NPs between the TiO_2 crystallite. The similar TEM observation on Au NPs incorporated TiO_2 crystallite is observed using one-step hydrothermal technique.[48] Therefore one-step electrospinning coating of TiO_2-Au directly onto the substrates result in effective dispersion of Au NPs in between TiO_2 crystallite instead of decorating on the surface.[49]

The chemical environment of TiO_2 NFs before and after Au NPs incorporation was studied by an X-ray photoelectron spectrometer (XPS), and the results are presented in **Fig.2**. From **Fig. 2a**, sharp shoulders observed at 458.8 and 464.6 eV corresponds to $Ti2p_{3/2}$ and $Ti2p_{5/2}$ orbital and are further shifted ~0.4 eV towards the lower binding energy region upon Au NPs incorporation. The atomic ratio of Ti, O and Au elements were estimated from XPS results (see supporting information Table T1). The asymmetric nature of O1s peak is separated into symmetric multiple peaks using Gaussian transformation fitting after background correction (See supporting information **Fig.S3**). The quantity of Ti is reduced from 57.3 to 50.6 % after Au incorporation, implies the

diffusivity of Au NPs at TiO_2 fiber and occupy in between TiO_2 as is observed from TEM image (Fig. 1g). Wang *et al* reported similar Ti2p peak shift in Ag NP incorporated TiO_2.[50] The O1s core spectra of pristine and Au incorporated TiO_2 is presented in Fig.2b. In TiO_2, three significant peaks (Fig.S3a) were identified at 529.7, 530.6, and 531.6 eV, where the first two peaks are assigned to lattice oxygen bound to Ti^{4+} and the third peak is attributed to hydroxyl groups of TiO_2. After Au NPs incorporation, a small peak was noticed at 532.2 eV inferring the possibility of water molecules adsorbed on TiO_2.[51] This enhanced hydrophilic property of TiO_2-Au HNFs is anticipated to result in high photocatalytic activity. The presence of Au at TiO_2 and their bonding nature with TiO_2 is further examined from Au 4f core spectra (Fig.2c). The strong shoulders appeared at 83.3 and 87.0 eV are assigned to $Au4f_{7/2}$ and $Au4f_{5/2}$ respectively.[52, 53]

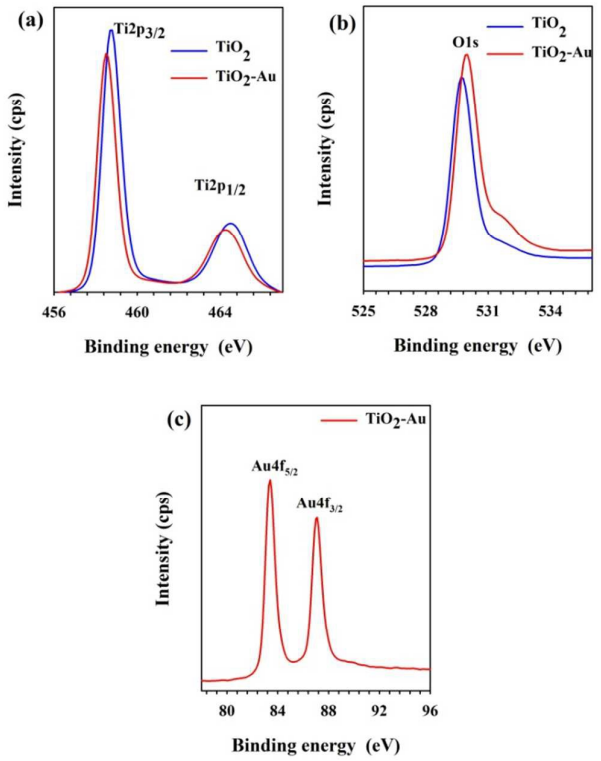

Figure 2. XPS results of TiO_2-Au electrodes (a) Ti2p core spectra (b) O1s core spectra (c) Au4f core spectra.

The quantity of Au is estimated from **Fig.2c** and is found to be 7.59% and the atomic ratio of Au/Ti is 0.15. The first peak $Au4f_{7/2}$ at 83.3 eV represents Au^0 bound at an oxygen vacancy (O^-) in the form of Au-$V^{\bullet\bullet}$.[54] It is known that oxygen vacancies formed in TiO_2 during sintering treatment act as Au nucleation sites.[55] The electrons initially belonging to the O_2^- ions contribute partially to the bond formation between Au and defect site. Thus the binding energy of this Au-$V^{\bullet\bullet}$ state is decreased by a negative charge transfer from the defective TiO_2 surface to the Au. Therefore the binding energy between TiO_2 and Au through oxygen vacancies plays a crucial role in catalysis reaction and charge transfer. The optical absorption spectra (Kulbelka-Munk) of both TiO_2 and TiO_2-Au HNFs are shown in **Fig.3**. The K-M absorption of TiO_2 shows the strong absorption peak around 375 nm which is attributed to the absorption of titania. After the inclusion of Au NPs in TiO_2, a strong absorption shoulder around 550 nm was observed, corresponding to the SPR band of Au NPs. The broad absorption peak indicates that the in-situ formation of Au NPs in TiO_2 nanofibrous network resulted in the formation of randomly size-distributed Au NPs.

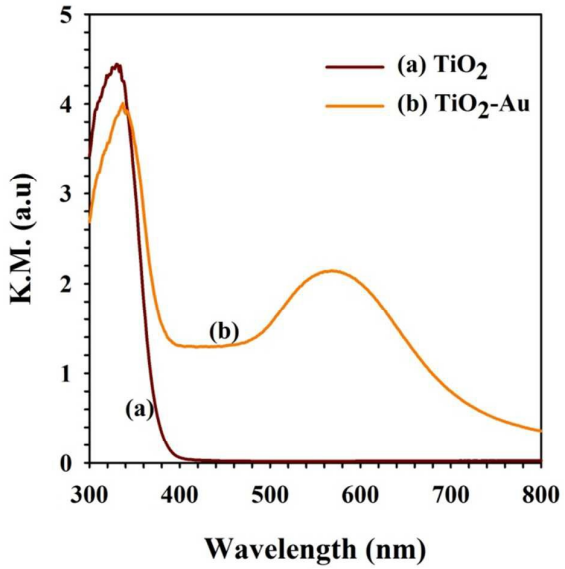

Figure 3. Optical absorbance spectra (Kulbelka-Munk) of TiO_2 and TiO_2-Au electrodes.

To investigate the photoelectrocatalytic property of pristine TiO_2 and TiO_2-Au HNFs, the J-V plots were recorded using standard three electrode systems. **Fig.4a** shows the typical J-V plots of TiO_2 NFs electrode in dark and light. The observed current density under light illumination was nearly 50 times higher than the dark current, which could be attributed to the photogenerated charge careers in pristine TiO_2. Similar response was observed for TiO_2-Au HNFs electrode under light illumination (**Fig.4b**). The photoholes assisted photoelectrocatalytic oxidation ability of pristine TiO_2 and TiO_2-Au HNFs was analyzed by adding 0.5 mM GSH in the electrolyte. As discussed earlier in **Scheme 1**, it is anticipated that the successful PEC oxidation of GSH into GSSG might enhance the photocurrent. Thus the enhancement of photocurrent in this system can be directly related to the PEC ability of TiO_2 and TiO_2-Au HNFs towards GSH bioanalysis. It is observed from **Fig.4a** that addition of 0.5 mM GSH resulted a negligible increase in photocurrent at TiO_2 NFs electrode,

which can be attributed to the poor photogenerated charge carrier separation at electrode/electrolyte interfaces and/or inadequate adsorption of GSH at TiO_2/electrolyte interface.

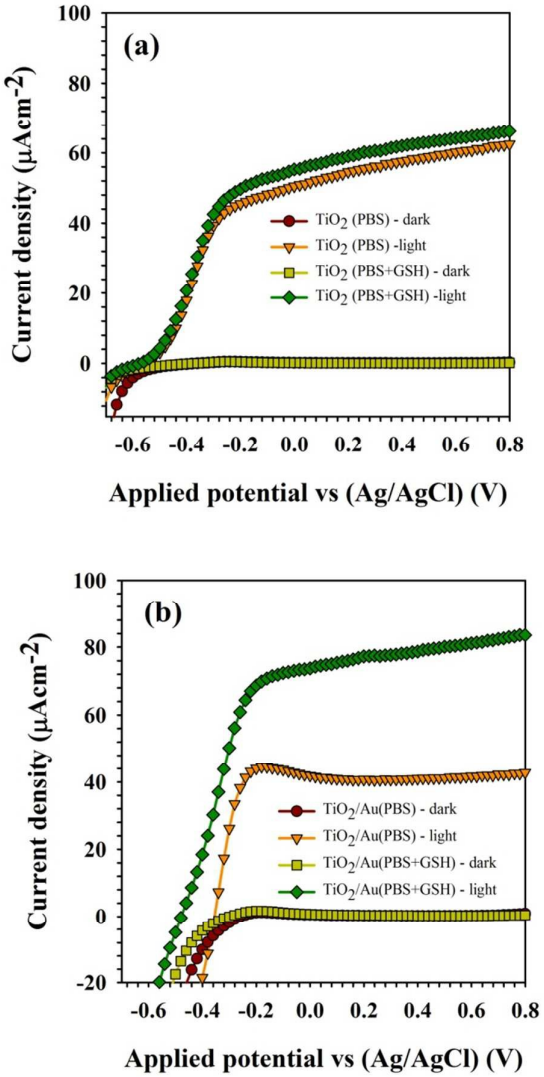

Figure 4. J-V plots of (a) TiO_2 and (b) TiO_2/Au composite electrodes. The measurements were carried out using PBS aqueous electrolyte. 0.5 mM GSH is used in the electrolyte. The simulated solar light is used for illumination (100 $mWcm^{-2}$).

In striking contrast, the addition of 0.5 mM GSH drastically improved the photocurrent generation by a factor of two (42.2 μAcm^{-2} to 84.4 μAcm^{-2}) at TiO_2-Au HNFs. This improvement may originate from Au NPs inclusion at TiO_2 by several reasons: (a) increasing the visible light reception at TiO_2 through light scattering or SPR effect (b) promoting charge carrier separation at TiO_2/Au interfaces and (c) high affinity of GSH molecules towards Au. Furthermore, it is observed that the onset potential of PEC GSH oxidation at TiO_2 NFs was observed at -0.35 V. The negative shift of the onset potential (-0.47 V vs Ag/AgCl) observed at TiO_2-Au HNFs, infers that Fermi level pinning at TiO_2/Au interfaces favor the photogenerated charge carrier separation. This negative potential of PEC GSH oxidation at TiO_2-Au HNFs electrode compared to TiO_2 NFs electrode is beneficial for the elimination of interference from other coexisting reductive species in the real time sample. Further increasing the applied potential higher than -0.25 V Ag/AgCl at TiO_2 and TiO_2-Au electrode shows no change in the photocurrent generation, implying the saturation of GSH oxidation at this potential.

In order to ensure the possibility of contributing additional electrons from Au NPs to TiO_2 through plasmonic effect (550 nm) for GSH oxidation, the PEC studies were performed using UV-cut off filter (400 nm) (JV plots not presented). It is well known that the UV-cut filter will block the visible light at 400 nm and thus restrict the TiO_2 from photoexcitation process, allowing the possibility of estimating the contribution of Au NPs in PEC process. The TiO_2-Au HNFs showed very negligible photocurrent generation after blocking the visible light at 400 nm (**Fig.S4**). This clearly depicts that no plasmonic effect was observed in this system.

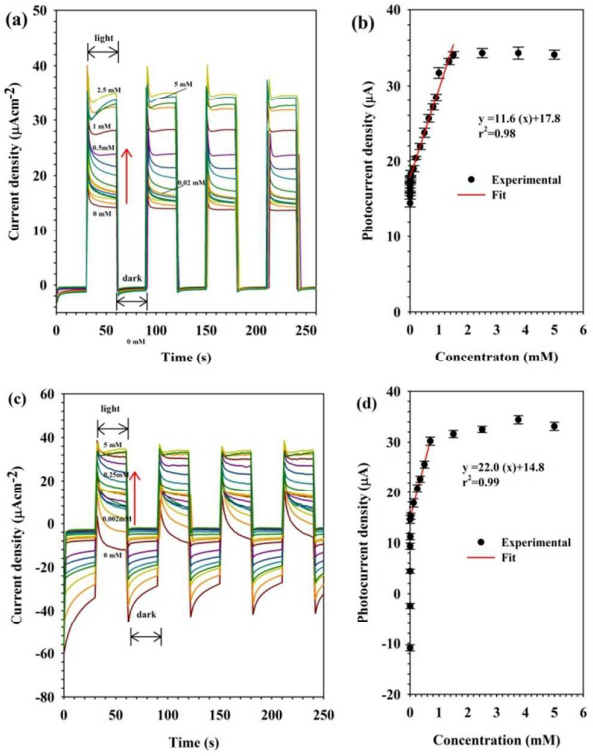

Figure 5. Chronoamperometry plots of PEC GSH bioanalysis using (a) TiO_2 and (c) TiO_2-Au photoanodes; liner fit relation between photocurrent generation and GSH concentration at different photoelectrodes (b) TiO_2 and (d) TiO_2-Au photoanodes. The measurements were carried out at -0.33 V vs (Ag/AgCl) using PBS aqueous electrolyte. The simulated solar light is used for illumination (100 $mWcm^{-2}$).

It is also significant discussing the interaction between the anode material and GSH biomolecules that could provide new insights into both selectivity and sensitivity. The biomolecule adsorption onto electrode can be qualitatively analyzed by dark current measurements at TiO_2 and TiO_2-Au electrodes in the presence and absence of GSH biomolecules. **Fig.S5** shows the J-V plots measured at dark condition. The high dark current observed at TiO_2-Au electrode compare to pristine TiO_2 electrode is attributed to the Schottky junction formation. Further inclusion of GSH molecules in PBS electrolyte was found to lower the dark current. This implies the GSH molecules adsorption on electrode, which serve as passivation layer to impede the electron from reacting with electrolyte directly. Such GSH adsorption onto electrode may lead to high PEC oxidation and thus produces significant difference in PEC current generation in **Fig.4b**. This effective interaction between GSH and Au surface may attributed to the formation of Au-x (x= N, O and S), through attracting thiol groups or intramolecular backbone hydrogen bonding of GSH.[56] The predominant interaction mechanism between GSH and Au was verified by using a GSH derivative that lacks hydrogen bonding e.g. glutathione disulfide (GSSG). **Fig.S6a** shows the chronoamperometric response of TiO_2-Au electrode in the presence of equal amounts of GSH and GSSG. It is found that the photocurrent generated for GSH at TiO2-Au electrode is twice than that of GSSG. This clearly indicates that the intramolecular backbone hydrogen bonding of GSH with Au and thus "hydrogen bonding" mechanism is dominating in this system.

On the basis of these observations, we have further explored the photoelectrocatalytic biosensing ability of TiO_2 and TiO_2-Au HNF electrodes using chronoamperometric measurements. **Fig.5a** shows the chronoamperometric response of TiO_2 electrode obtained by successive addition of GSH under -0.33 V vs (Ag/AgCl) applied potential. Upon visible light irradiation, the photocurrent density at TiO_2 NFs electrode increases from 0 to 28 μAcm^{-2}. Further, these TiO_2 NFs electrode responded quickly to the successive addition of GSH with a steady photocurrent increase up to 1.5 mM. The photocurrent reaches the saturation level at 2 mM GSH after which any further increase in GSH concentration does not produce any change in the photocurrent production (**Fig.5b** The limit of detection, LOD, defined as $I_{BLANK} + 3s_{BLANK}$, for pristine TiO_2 NF was estimated to be 17 µM with a broad detection range between 0 to 2. mM, A wide linear detection range between 0.025 to 1.5 mM was obtained for GSH detection. The detection range of pristine TiO_2 NFs (our work) is comparable with porphyrin modified TiO_2.[33] On the other hand, TiO_2-Au HNFs shows high dark current ~- 40 $\mu A.cm^{-2}$ compare to pristine TiO_2 HNF at similar applied potential (-0.33 V vs (Ag/AgCl) (**Fig.5c**). This might be attributed to the electron passage from TiO_2 to electrolyte through Au NPs schottky junction as is discussed above (**Figure S4**). This dark current value found to be decrease by increasing GSH concentration in the electrolyte. This implies that the GSH molecules are adsorbed onto Au NPs surface and thus impede the electron passage from Au NPs to electrolyte. **Fig.5d** shows the calibration plot of photocurrent density vs GSH concentration at TiO_2-Au HNFs electrode. The photocurrent density was found to increase steadily with the successive addition of GSH. A linear detection range between 0.022 to 0.7 mM of GSH is observed with least detection of 0.002 mM GSH using TiO_2-Au electrode.

Our scientific observation indicates indicates that both TiO_2 and TiO_2-Au HNF electrodes shows comparable linear detection range in our system. It is worth mentioning that the response range observed in our system was wider than the earlier reports using electrogenerated chemiluminescence of quantum dots (0.024-0.214 mM),[22] the fluorometric method (0.025-0.25 mM),[57] and surface-enhanced Raman scattering (0.1-0.8 µM). The detection limit observed in our work (0.002 mM) is lower than the previous methods; it is worth mentioning that the improved upper limit of detection (> 5 mM) authenticates our photoelectrochemical detection of GSH more suitable for biological samples, because the normal level of GSH in human fluids is in the range of 0.1-10 mM.[33, 58] The selectivity of PEC detection of GSH using TiO_2 NFs and TiO_2-Au HNFs electrode was confirmed by measuring the response in the presence of interfering molecules. **Fig.6** shows the chronoamperogram of TiO_2 NFs and TiO_2-Au HNFs recorded with the interference of ascorbic acid and glucose.

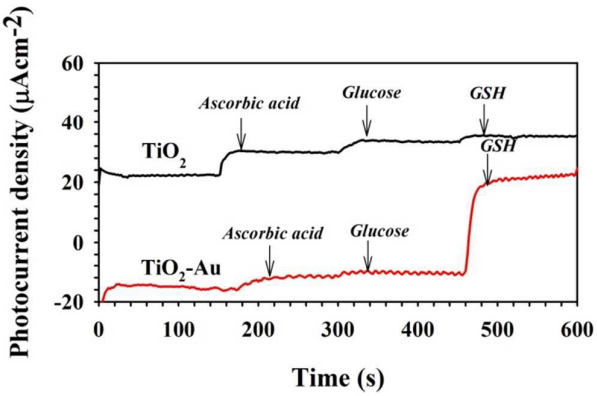

Figure 6. Chronoamperometry plots showing the selectivity of TiO_2 (black line) and TiO_2-Au HNFs (red line). The measurements were carried out using PBS aqueous electrolyte. The simulated solar light is used for illumination (100 $mWcm^{-2}$).

It is found that the photocurrent response of TiO_2 NFs is affected by the presence of ascorbic acid and glucose. Strikingly, the TiO_2-Au HNFs electrodes show very negligible change in the photocurrent response with the addition of ascorbic acid and glucose, resulting in a very distinct predominant response exclusively to GSH oxidation. Though pristine TiO_2 electrodes show wide range of GSH linear detection comparable with TiO_2-Au electrode, it is inferior in GSH selectivity in the presence of other biological species. The high specificity of TiO_2-Au HNFs towards PEC GSH oxidation makes it a potential candidate for the real time PEC GSH analysis. Moreover, electrospun derived fibrous coating can be directly implemented as "ready-to-use" type dip and read biosensors[59] or applied bias driven electrochemical

biosensors.[60] However, it is worth mentioning that the interference analysis with cysteine shows noticeable interference during the detection of GSH at TiO_2-Au electrode (**Fig.S6b**). This is possibly due to the similar oxidation potential of cysteine and GSH. This can be addressed by introducing the intermediate molecules such as catechol which undergoes an electrochemical oxidation to form an *o*-quinone that can mediate in the reaction with a thiol, RSH, to form RSSR to eliminate the interference.[61, 62] In detailed examination is needed to address this issue and is under progress.

Conclusions

The electrospun TiO_2-Au HNFs display enhanced photoelectrocatalytic activity towards GSH bioanalysis when compared to the pristine TiO_2 NFs under identical conditions. The electrochemical analysis on nano-bio interface implies that the presence of Au NPs improve the adsorption of GSH molecules onto the electrode surface due to their higher affinity towards thiol molecules. Thus, the process of GSH adsorption onto TiO_2-Au surface readily promotes the PEC oxidation of GSH and thus results wide GSH detection range with high specificity towards the presence of interference molecules such as ascorbic acid and glucose. As a result, TiO_2-Au HNFs showed a linear detection range from 22 µM to 0.7 mM with high selectivity of GSH compared to pristine TiO_2 electrode. The experimental results suggested that the single-step TiO_2-Au HNF fabrication technique reduces the material consumption than multi-step metal-metal oxide composite preparation techniques and thus, anticipated to be attractive in wide range of electrochemical and photoelectrochemical devices. The shape controlled TiO_2-Au HNF without fiber aggregation could be futuristic in biosensing application with wide range of molecule detection. The analysis of charge transfer kinetics at electrode/electrolyte interfaces is significant to extend the selectivity and sensitivity of the electrodes.

Experimental

Electrospun TiO_2-Au composite NFs fabrication. The TiO_2 and TiO_2-Au HNFs were prepared using electrospining technique as follows: Typically, titanium tetraisopropoxide ($Ti(OiPr)_4$, Aldrich, 3 g) was mixed with acetic acid (2 mL) and ethanol (2 mL) and stirred for 10 minutes. The above solution was added to ethanol (3 mL) that contains polyvinyl pyrrolidone (PVP) (Aldrich, Mw ≈1300000, Aldrich, 0.3 g) and is stirred uniformly for 20 min. In case of TiO_2-Au composite NFs, a known amount of tetrachloroaurate trihydrate ($HAuCl_4.3H_2O$, sigma Aldrich, 0.03 g) was added to the titania precursor solution and mixed completely using magnetic stirrer for 20 min. The resultant mixture is loaded into electrospinning syringe. The solution feeding rate to nozzle is controlled with automatic microcontroller at the rate of 1.0 mL/h. The applied voltage of 12 KV is given to the nozzle. The distance between the collector and nozzle is maintained to be 12 cm for generating nanofibers. The electro spinning process is conducted at ambient condition. After this process, the fibrous samples are subsequently treated with ethanol to improve their physical contact with substrate. Finally, TiO_2 and TiO_2-Au NFs are sintered at 500 ºC for 1 h under air atmosphere.

Characterization. The surface morphology of TiO_2 and TiO_2-Au NFs was characterized using a field emission scanning electron microscope (FE-SEM, JSM 7600F, JEOL, Tokyo, Japan) and a field emission transmission electron microscope (HR-TEM, JEM-2100F, JEOL, Tokyo, Japan). The chemical environment of pristine TiO_2 and TiO_2-Au NFs was analyzed by x-ray photoelectron spectroscopy (XPS) using an angular resolved electron analyzer with a monochromated Al Kα source (AXIS Nova KRATOS ANALYTICAL). The optical diffuse reflectance spectra of the electrodes were recorded in the range of 350–900 nm using a V670 JASCO UV-Vis spectrophotometer. The absorbance of the electrodes was estimated directly using Kulbelga-Munk relation with in-built software from JASCO UV-Vis spectrometer.

Photoelectrochemical measurements. The PEC analysis was done using a three electrode configuration. The as-prepared TiO_2 and TiO_2-Au NFs electrodes (electrode area 1 cm^2) were used as the working electrode, Ag/AgCl as the reference and Pt foil as the counter electrode. 0.1 M phosphate buffered saline (PBS) (Sigma Aldrich, pH=7.1) was used as the electrolyte for all PEC measurements. Cyclic voltammograms were recorded using the advanced potentiostat (PGSTAT-30 from Autolab) with the scanning rate 50 mV/s. The photocurrent measurements were recorded using a solar simulator with a 300 W xenon arc-lamp (Asahi Spectra- HAL 320 W). The light intensity (100 $mWcm^{-2}$) was calibrated using a silicon photodiode. The chronoamperometry analysis was carried out for TiO_2 and TiO_2-Au NFs and was tested with different glutathione concentration.

Acknowledgements

One of the authors, P.S., appreciates JSPS for providing the post doctoral fellowship (ID:13374).

References

1. A. Fujishima and K. Honda, *Nature*, 1972, 238, 37-38.
2. P. Rodenas, T. Song, P. Sudhagar, G. Marzari, H. Han, L. Badia-Bou, S. Gimenez, F. Fabregat-Santiago, I. Mora-Sero, J. Bisquert, U. Paik and Y. S. Kang, *Advanced Energy Materials*, 2013, 3, 176-182.
3. P. Sudhagar, K. Asokan, E. Ito and Y. S. Kang, *Nanoscale*, 2012, 4, 2416-2422.
4. P. Sudhagar, A. Devadoss, T. Song, P. Lakshmipathiraj, H. Han, V. V. Lysak, C. Terashima, K. Nakata, A. Fujishima, U. Paik and Y. S. Kang, *Physical Chemistry Chemical Physics*, 2014, 16, 17748-17755.

5. W.-W. Zhao, J.-J. Xu and H.-Y. Chen, *Chemical Society Reviews*, 2015, 44, 729-741.
6. A. Devadoss, P. Sudhagar, S. Das, S. Y. Lee, C. Terashima, K. Nakata, A. Fujishima, W. Choi, Y. S. Kang and U. Paik, *ACS Applied Materials & Interfaces*, 2014, 6, 4864-4871.
7. Z. Yue, F. Lisdat, W. J. Parak, S. G. Hickey, L. Tu, N. Sabir, D. Dorfs and N. C. Bigall, *ACS Applied Materials & Interfaces*, 2013, 5, 2800-2814.
8. E. Golub, A. Niazov, R. Freeman, M. Zatsepin and I. Willner, *The Journal of Physical Chemistry C*, 2012, 116, 13827-13834.
9. W.-W. Zhao, J.-J. Xu and H.-Y. Chen, *Chemical Reviews*, 2014, 114, 7421-7441.
10. M. Salari, S. H. Aboutalebi, A. Aghassi, P. Wagner, A. J. Mozer and G. G. Wallace, *Physical Chemistry Chemical Physics*, 2015, 17, 5642-5649.
11. S. Y. Chae, P. Sudhagar, A. Fujishima, Y. J. Hwang and O.-S. Joo, *Physical Chemistry Chemical Physics*, 2015, 17, 7714-7719.
12. J. Tang, J. Li, P. Da, Y. Wang and G. Zheng, *Chemistry – A European Journal*, 2015, DOI: 10.1002/chem.201406643, n/a-n/a.
13. N. H. P. Cnubben, I. M. C. M. Rietjens, H. Wortelboer, J. van Zanden and P. J. van Bladeren, *Environmental Toxicology and Pharmacology*, 2001, 10, 141-152.
14. M. Gutscher, A.-L. Pauleau, L. Marty, T. Brach, G. H. Wabnitz, Y. Samstag, A. J. Meyer and T. P. Dick, *Nat Meth*, 2008, 5, 553-559.
15. R. Deng, X. Xie, M. Vendrell, Y.-T. Chang and X. Liu, *Journal of the American Chemical Society*, 2011, 133, 20168-20171.
16. H. Liu, H. Wang, S. Shenvi, T. M. Hagen and R.-M. Liu, *Annals of the New York Academy of Sciences*, 2004, 1019, 346-349.
17. F. Pinnen, P. Sozio, I. Cacciatore, C. Cornacchia, A. Mollica, A. Iannitelli, E. D'Aurizio, A. Cataldi, S. Zara, C. Nasuti and A. Di Stefano, *Archiv der Pharmazie*, 2011, 344, 139-148.
18. R. Anandan, B. Ganesan, T. Obulesu, S. Mathew, K. K. Asha, P. T. Lakshmanan and A. A. Zynudheen, *Cell Stress and Chaperones*, 2013, 18, 121-125.
19. N. D. Goncharova, A. V. Shmaliy, V. Y. Marenin and S. A. Smelkova, *Bull Exp Biol Med*, 2007, 144, 730-733.
20. D. Y. Wong, Y. L. Hsiao, C. K. Poon, P. C. Kwan, S. Y. Chao, S. T. Chou and C. S. Yang, *Cancer Lett*, 1994, 81, 111-116.
21. C.-C. Yeh, M.-F. Hou, S.-H. Wu, S.-M. Tsai, S.-K. Lin, L. A. Hou, H. Ma and L.-Y. Tsai, *Cell Biochemistry and Function*, 2006, 24, 555-559.
22. Y. Wang, J. Lu, L. Tang, H. Chang and J. Li, *Analytical Chemistry*, 2009, 81, 9710-9715.
23. J. C. Harfield, C. Batchelor-McAuley and R. G. Compton, *Analyst*, 2012, 137, 2285-2296.
24. L.-Y. Niu, Y.-S. Guan, Y.-Z. Chen, L.-Z. Wu, C.-H. Tung and Q.-Z. Yang, *Journal of the American Chemical Society*, 2012, 134, 18928-18931.
25. X. Chen, Y. Zhou, X. Peng and J. Yoon, *Chemical Society Reviews*, 2010, 39, 2120-2135.
26. M. H. Pournaghi-Azar and F. Ahour, *Journal of Electroanalytical Chemistry*, 2008, 622, 22-28.
27. J. Tang, Y. Wang, J. Li, P. Da, J. Geng and G. Zheng, *Journal of Materials Chemistry A*, 2014, 2, 6153-6157.
28. J. Bai and B. Zhou, *Chemical Reviews*, 2014, 114, 10131-10176.
29. D. Chen, H. Zhang, X. Li and J. Li, *Analytical chemistry*, 2010, 82, 2253-2261.
30. X. Zeng, J. Bao, M. Han, W. Tu and Z. Dai, *Biosensors and Bioelectronics*, 2014, 54, 331-338.
31. J. Tang, Y. Zhang, B. Kong, Y. Wang, P. Da, J. Li, A. A. Elzatahry, D. Zhao, X. Gong and G. Zheng, *Nano Letters*, 2014, 14, 2702-2708.
32. Q. Han, K. Wang, L. Xu, X. Yan, K. Zhang, X. Chen, Q. Wang, L. Zhang and R. Pei, *Analyst*, 2015, 140, 4143-4147.
33. W. Tu, Y. Dong, J. Lei and H. Ju, *Analytical Chemistry*, 2010, 82, 8711-8716.
34. J. Tang, B. Kong, Y. Wang, M. Xu, Y. Wang, H. Wu and G. Zheng, *Nano Letters*, 2013, 13, 5350-5354.
35. Y. Nakato, K. Ueda, H. Yano and H. Tsubomura, *The Journal of Physical Chemistry*, 1988, 92, 2316-2324.
36. V. Subramanian, E. Wolf and P. V. Kamat, *The Journal of Physical Chemistry B*, 2001, 105, 11439-11446.
37. F. P. García de Arquer, A. Mihi, D. Kufer and G. Konstantatos, *ACS Nano*, 2013, 7, 3581-3588.
38. S. Mubeen, G. Hernandez-Sosa, D. Moses, J. Lee and M. Moskovits, *Nano Letters*, 2011, 11, 5548-5552.
39. C. Clavero, *Nat Photon*, 2014, 8, 95-103.
40. M. D. Brown, T. Suteewong, R. S. S. Kumar, V. D'Innocenzo, A. Petrozza, M. M. Lee, U. Wiesner and H. J. Snaith, *Nano Letters*, 2011, 11, 438-445.
41. G. Chen, J. Wang, C. Wu, C.-z. Li, H. Jiang and X. Wang, *Langmuir*, 2012, 28, 12393-12399.
42. J. B. Priebe, J. Radnik, A. J. J. Lennox, M.-M. Pohl, M. Karnahl, D. Hollmann, K. Grabow, U. Bentrup, H. Junge, M. Beller and A. Brückner, *ACS Catalysis*, 2015, 5, 2137-2148.
43. P. Sudhagar, T. Song, A. Devadoss, J. W. Lee, M. Haro, S. Gimenez, C. Terashima, V. V. Lysak, J. Bisquert, A. Fujishima and U. Paik, *Physical Chemistry Chemical Physics*, 2015, DOI: 10.1039/c5cp01175b.
44. H. Zhao, B. Lu, J. Xu, E. Xie, T. Wang and Z. Xu, *Nanoscale*, 2013, 5, 2835-2839.
45. H.-g. Wang, Y.-h. Li, W.-q. Liu, Y.-c. Wan, Y.-w. Li and Q. Duan, *RSC Advances*, 2014, 4, 23125-23130.
46. P. Sudhagar, V. Gonzalez-Pedro, I. Mora-Sero, F. Fabregat-Santiago, J. Bisquert and Y. S. Kang, *Journal of Materials Chemistry*, 2012, 22, 14228-14235.
47. P. S. Kumar, S. A. S. Nizar, J. Sundaramurthy, P. Ragupathy, V. Thavasi, S. G. Mhaisalkar and S. Ramakrishna, *Journal of Materials Chemistry*, 2011, 21, 9784-9790.
48. G. Zhang, Z. Zhao, H. Tan, H. Zhao, D. Qu, M. Zheng, W. Yu and Z. Sun, *RSC Advances*, 2015, 5, 21237-21241.
49. J. Huang, T. Kunitake and S.-y. Onoue, *Chemical Communications*, 2004, DOI: 10.1039/b401071j, 1008-1009.
50. S. Wang, H. Qian, Y. Hu, W. Dai, Y. Zhong, J. Chen and X. Hu, *Dalton Transactions*, 2013, 42, 1122-1128.
51. N. Kruse and S. Chenakin, *Applied Catalysis A: General*, 2011, 391, 367-376.
52. A. Y. Klyushin, T. C. R. Rocha, M. Havecker, A. Knop-Gericke and R. Schlogl, *Physical Chemistry Chemical Physics*, 2014, 16, 7881-7886.
53. E. A. Willneff, S. Braun, D. Rosenthal, H. Bluhm, M. Hävecker, E. Kleimenov, A. Knop-Gericke, R. Schlögl and S. L. M. Schroeder,

Journal of the American Chemical Society, 2006, 128, 12052-12053.
54. X.-Q. Gong, A. Selloni, O. Dulub, P. Jacobson and U. Diebold, *Journal of the American Chemical Society*, 2008, 130, 370-381.
55. Z. Jiang, W. Zhang, L. Jin, X. Yang, F. Xu, J. Zhu and W. Huang, *The Journal of Physical Chemistry C*, 2007, 111, 12434-12439.
56. Z. Aliakbar Tehrani, Z. Jamshidi, M. Jebeli Javan and A. Fattahi, *The Journal of Physical Chemistry A*, 2012, 116, 4338-4347.
57. Z. Yao, X. Feng, C. Li and G. Shi, *Chemical Communications*, 2009, DOI: 10.1039/b912811e, 5886-5888.
58.D. P. Jones, J. L. Carlson, V. C. Mody Jr, J. Cai, M. J. Lynn and P. Sternberg Jr, *Free Radical Biology and Medicine*, 2000, 28, 625-635.
59. X. Ji, Z. Su, P. Wang, G. Ma and S. Zhang, *Analyst*, 2014, 139, 6467-6473.
60. K. Mondal, M. A. Ali, V. V. Agrawal, B. D. Malhotra and A. Sharma, *ACS Applied Materials & Interfaces*, 2014, 6, 2516-2527.
61. P. T. Lee, D. Lowinsohn and R. G. Compton, *Electroanalysis*, 2014, 26, 1488-1496.
62. P. T. Lee, D. Lowinsohn and R. G. Compton, *Analyst*, 2014, 139, 3755-3762.

Graphical Abstract

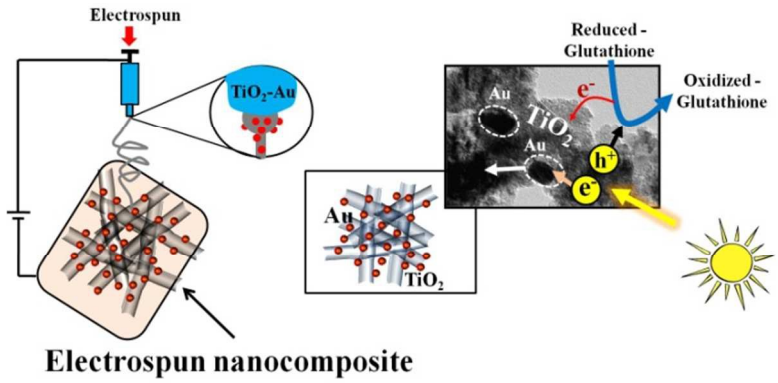

One-step electrospun Au nanoparticle decorated TiO_2 nanofiber membrane served as effective photoanode for highly selective glutathione analysis through photoelectrocatalytic oxidation process.